Supporting Information

Precise construction of symmetrically coordinated triatomic zirconium catalyst for efficient oxygen reduction

Anaer Husile, Tianmi Tang, Liyuan Xiao, Zhenlu Wang* and Jingqi Guan*

Institute of Physical Chemistry, National Demonstration Center for Experimental Chemistry Education, College of Chemistry, Jilin University, 2519 Jiefang Road, Changchun 130021, China. *Corresponding author. E-mail: wzl@jlu.edu.cn (Z.L. Wang), guanjq@jlu.edu.cn (J.Q. Guan)

Experimental Section

Synthesis of Zr_3 precursor

Zr_3 precursor was synthesized following a similar strategy reported by Wei et al.[1] 615 mg of isonicotinic acid was dissolved in 15 mL of H_2O and 200 mg of NaOH was added and stirred for 10 min to obtain a clear solution of system 1. The clear solution of system 2 was obtained by adding Cp_2ZrCl_2 (1.465 g) and 30 mL CH_2Cl_2 to another beaker. The clear solution of system 1 was added dropwise to system 2 under stirring, and stirred at 25 °C for 4 h, forming an emulsion suspension. The suspension was filtered, washed, and vacuum dried at 60 °C to obtain a white trinuclear zirconium metal precursor.

Synthesis of Zr_3/NG

100 mg of graphene oxide (GO) was dispersed in 80 mL of CH_3CH_2OH solution under stirring for 30 minutes. Then the trinuclear zirconium precursor was added and continually stirred for 1 h, and then the Zr_3-GO powder was obtained by rotary evaporation. The Zr_3-GO powder was pyrolyzed in a Joule heating rapid heating device in an NH_3 environment. Zr_3-n%-T-NG samples with different ratios (0.6%, 0.9%, 1.2%, 1.5%, 2.0%) at different temperatures (T = 1300 ^oC, 1400 ^oC and 1500 ^oC) were obtained.

Synthesis of Zr_1/NG

100 mg of GO and 3.1 mg of $ZrCl_4$ were uniformly dispersed in 80 mL of ethanol via an ultrasound-assisted method, and the Zr_1/GO powder was obtained by rotary evaporation. Using NH_3 as the nitrogen source, the powder was calcined in a Joule heating rapid thermal treatment device to obtain Zr_1/NG.

Synthesis of NG

Using NH_3 as the nitrogen source, GO was calcined at 1400 °C in a Joule heating rapid thermal treatment device, and the resulting material was denoted as NG.

Characterizations

The atomic distribution of zirconium in Zr_3/NG catalyst was analyzed by AC-HAADF-STEM (Spectra 300) and TEM (JEM-2100) combined with energy

dispersive X-ray spectroscopy. The catalyst's crystalline structure was characterized using powder X-ray diffraction (XRD-6100). Elemental composition and chemical states of Zr in Zr_3/NG were examined by XPS (Thermo ESCALAB 250 Xi). Zr K-edge X-ray absorption fine structure (XAFS) measurements were conducted at the BL11B beamline of Shanghai Synchrotron Radiation Facility.

Electrochemical measurements

The ORR performance was tested in an electrolytic cell containing 100 mL of 0.1 mol/L KOH solution. The ring-disk electrode (RDE) or rotating ring-disk electrode (RRDE) was used as the working electrode, Hg/HgO was used as the reference electrode, and the platinum electrode was used as the counter electrode. The powder catalyst of 2.0 mg was mixed with 200 mL of 0.25 wt.% Nafion solution and put into an ultrasonic cleaner for 30 minutes to obtain a homogeneous slurry. Subsequently, 8 μL of the slurry was uniformly deposited onto the working electrode. Before the test, pure O_2 or pure N_2 gas was introduced into the electrolyte to reach the saturation state of the solution for at least 30 min. After the test, we convert the obtained parameters into a reversible hydrogen electrode (RHE):

$$V_{RHE} = V_{Hg/HgO} + V^{\theta}_{Hg/HgO} + 0.0591pH$$

Using the RDE system, the linear sweep curve (LSV) test was performed at a scanning speed of 5 mV/s under the condition that both O_2 and N_2 reached saturation, and the cyclic voltammetry curve (CV) test was performed at a scanning speed of 50 mV/s and 100 mV/s, respectively.

ORR kinetic analysis was performed using the K-L equation:

$$\frac{1}{j}=\frac{1}{j_k}+\frac{1}{j_L}$$

j: measured current density, j_k: kinetically controlled current density, j_L: diffusion-controlled current density.

The electron transfer number and hydrogen peroxide yield were calculated by RRDE measurement:

$$H_2O_2(\%) = 200 \times \frac{\frac{I_r}{N}}{I_d + \frac{I_r}{N}}$$

$$n = 4 - \frac{2H_2O_2(\%)}{100}$$

I_d: disk current, I_r: ring current and N: ring electrode collection efficiency (N = 0.25).

ECSA is obtained by CV curves at different scanning rates. The formula is as follows:

$$ECSA = \frac{C_{dl}}{C_s}$$

C_s: standard specific capacitance (0.04 mF cm^{-2}).

Zn-air battery measurements

The performance of Zr_3/NG-based zinc-air battery was evaluated on a blue electric test system (LANHE CT2001A). The polished zinc sheet was used as the anode, and the carbon paper coated with catalyst was used as the cathode. The catalyst

slurry was prepared by mixing 100 μL of 1% Nafion/ethanol solution, 500 μL of ethanol and 2 mg of catalyst powder. The electrolyte is a mixed solution of 6M KOH and 0.2M $Zn(CH_3COO)_2$. The polarization curve was measured at a scan rate of 10 m V s^{-1}. The constant current charge/discharge cycle test was performed at a current density of 5 mA cm^{-2}, and each charge/discharge cycle lasted for 10 min.

DFT calculations

In this study, a series of theoretical calculations were carried out using the density functional theory (DFT) framework combined with the Vienna self-consistent simulation package (VASP) to explore the mechanism of ORR. All calculations are based on the generalized gradient approximation (GGA) and the Perdew-Burke-Ernzerhof (PBE) exchange-correlation functional. The electron-ion interaction is described by the projection enhanced wave (PAW) method. All calculations are spin-polarized to ensure an accurate description of the magnetic or electronic structure.

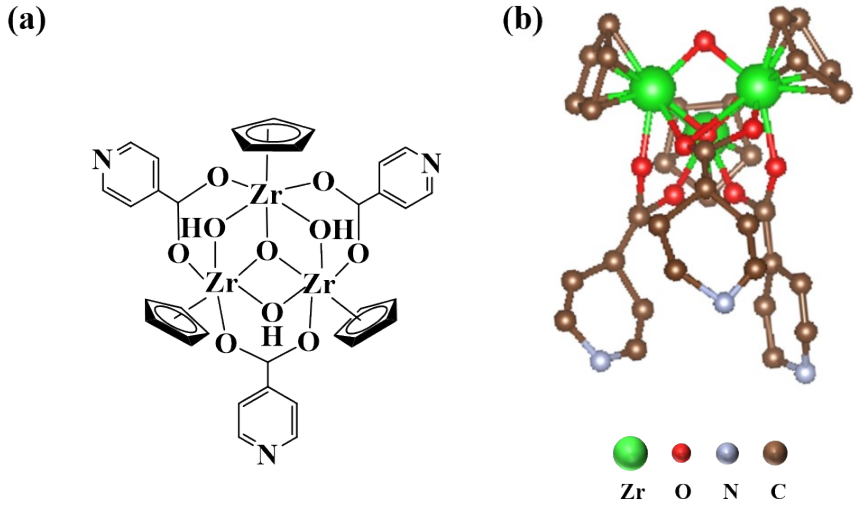

Figure S1. (a) The molecular structure of Zr_3 precursor. (b) Ball-stick model of Zr_3 precursor.

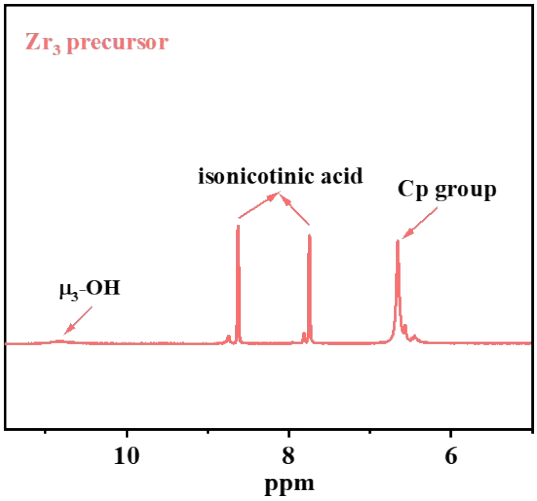

Figure S2. ^1H NMR spectrum of Zr_3 precursor.

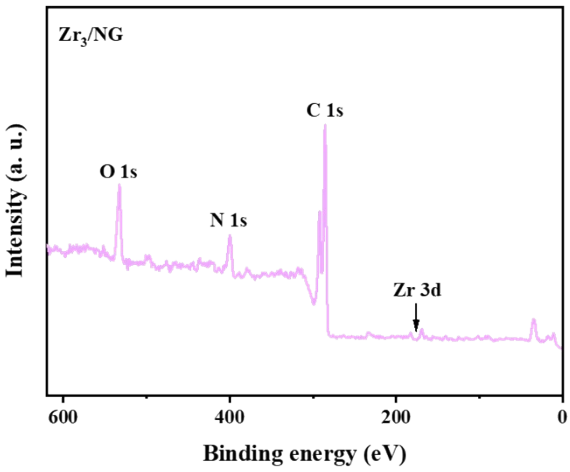

Figure S3. XPS survey spectrum of Zr_3/NG.

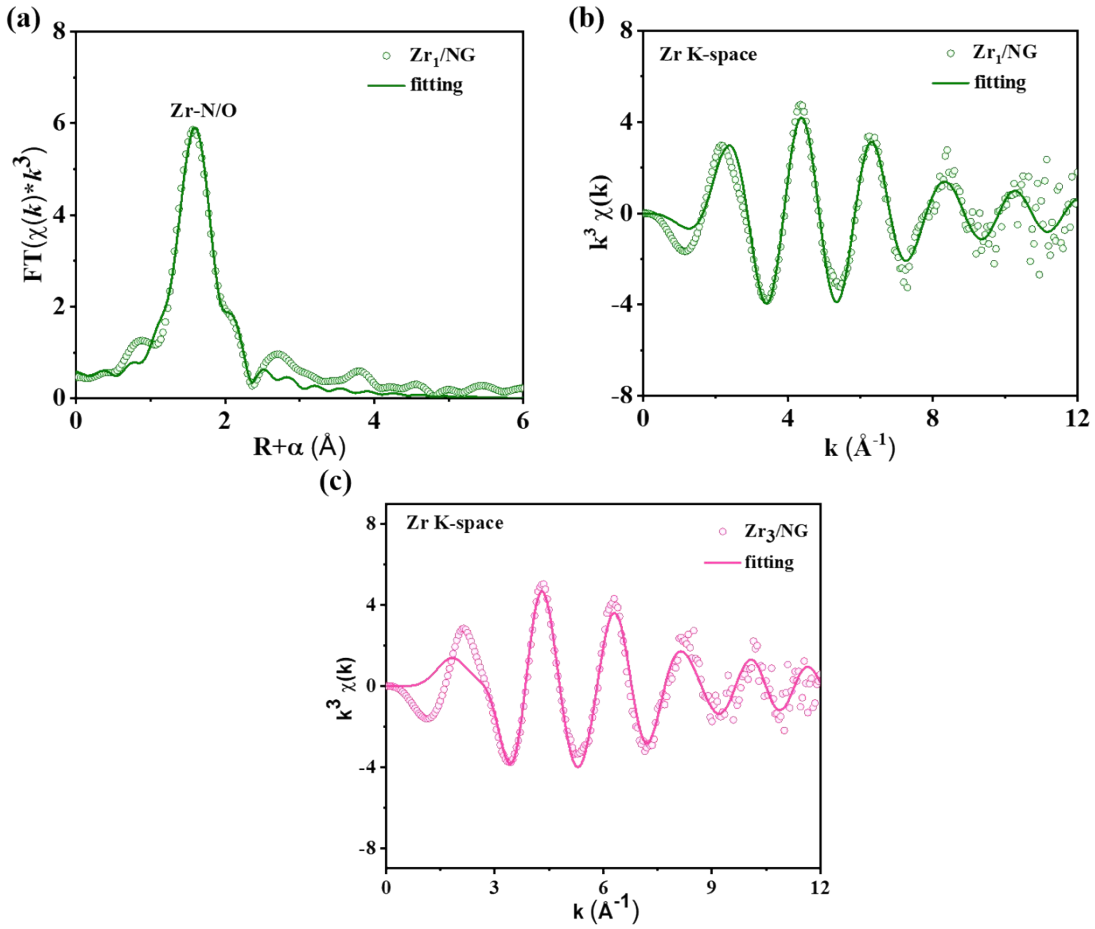

Figure S4. (a, b) FT-EXAFS of the R-space and k-space fitting curve for the Zr_1/NG.

(c) FT-EXAFS of the k-space fitting curve for the Zr_3/NG.

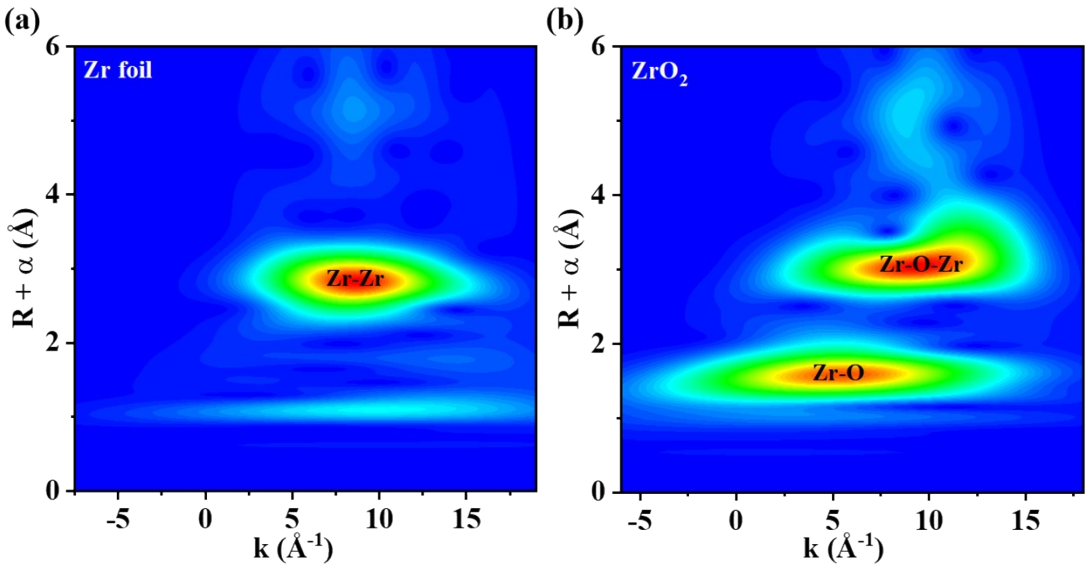

Figure S5. WT-EXAFS plots for Zr foil and ZrO_2.

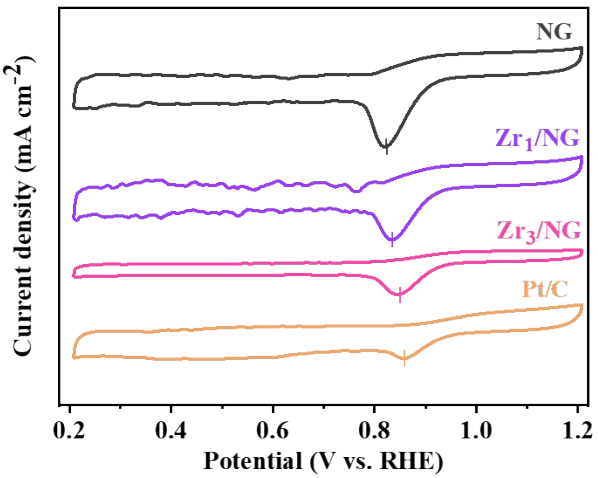

Figure S6. CV curves of Zr_3/NG, Zr_1/NG, NG and 20% Pt/C in O_2-saturated 0.1 M KOH at a sweep rate of 5 mV s^{-1}.

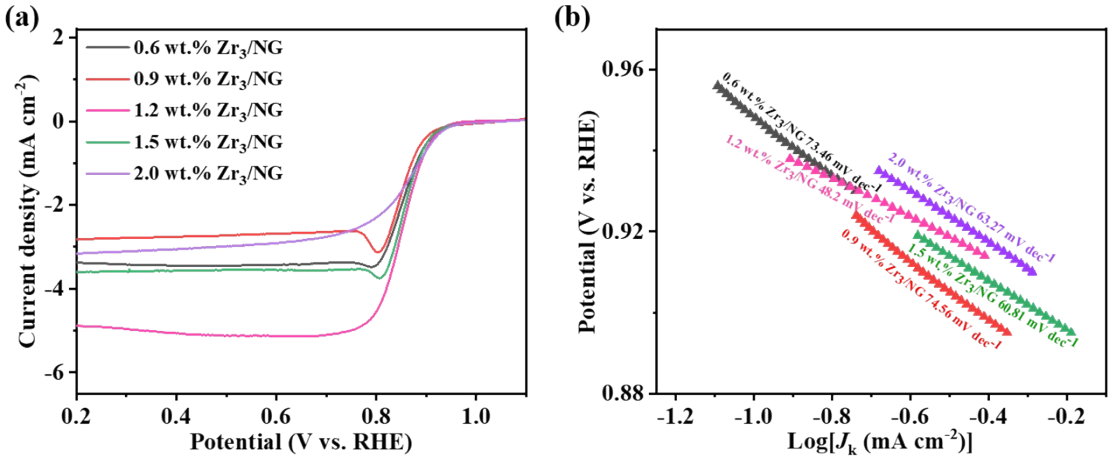

Figure S7. (a) Polarization curves of x wt.% Zr_3/NG-1400 at a rotation speed of 1600 rpm min^{-1}. (b) Tafel plots.

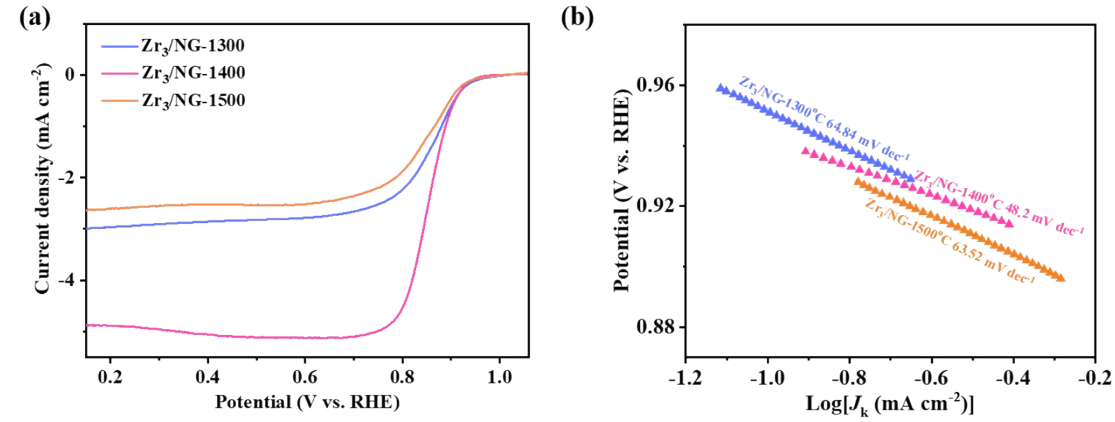

Figure S8. (a) Polarization curves ofZr_3/NG-T at a rotation speed of 1600 rpm min^{-1}. (b) Tafel plots.

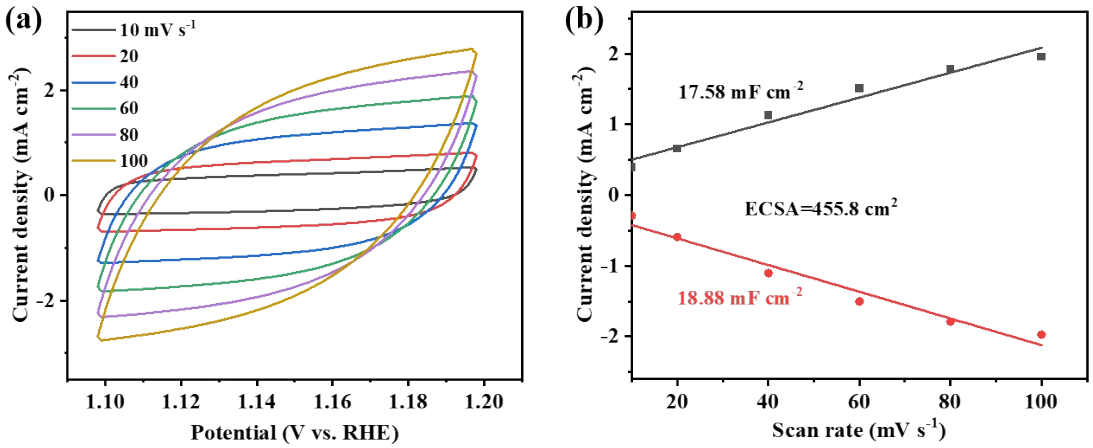

Figure S9. (a) CVs of Zr_3/NG measured in a non-Faradaic region at scan rate of 10 mV s^{-1}, 20 mV s^{-1}, 40 mV s^{-1}, 60 mV s^{-1}, 80 mV s^{-1}, and 100 mV s^{-1}. (b) Capacitive j vs scan rate.

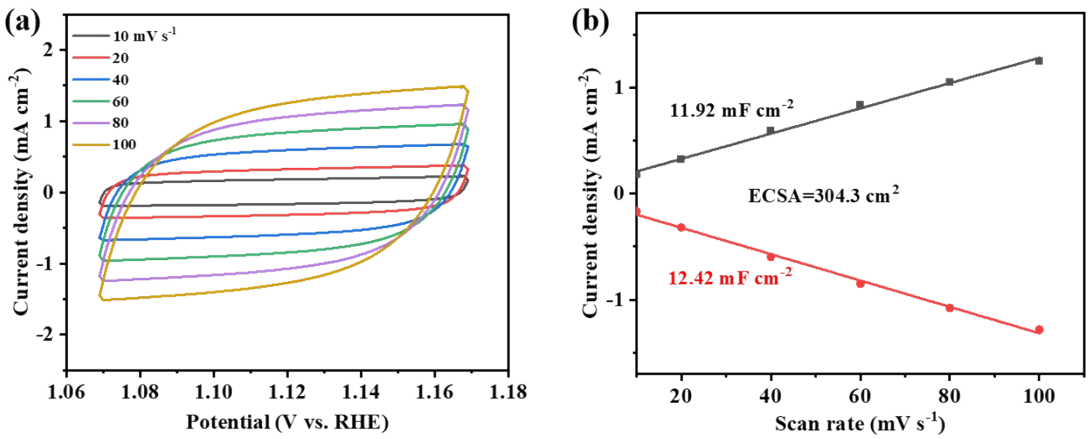

Figure S10. (a) CVs of Zr_1/NG measured in a non-Faradaic region at scan rate of 10 mV s^{-1}, 20 mV s^{-1}, 40 mV s^{-1}, 60 mV s^{-1}, 80 mV s^{-1}, and 100 mV s^{-1}. (b) Capacitive j vs scan rate.

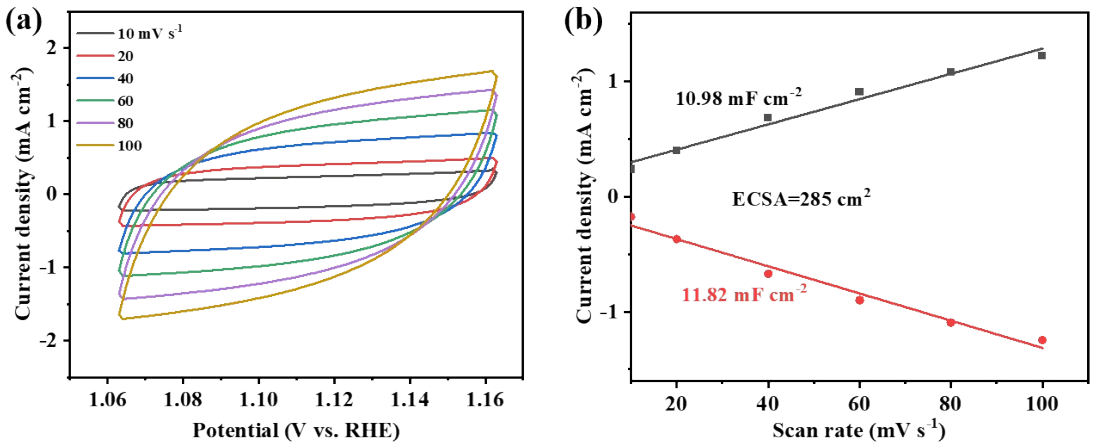

Figure S11. (a) CVs of Pt/C measured in a non-Faradaic region at scan rate of 10 mV s^{-1}, 20 mV s^{-1}, 40 mV s^{-1}, 60 mV s^{-1}, 80 mV s^{-1}, and 100 mV s^{-1}. (b) Capacitive j vs scan rate.

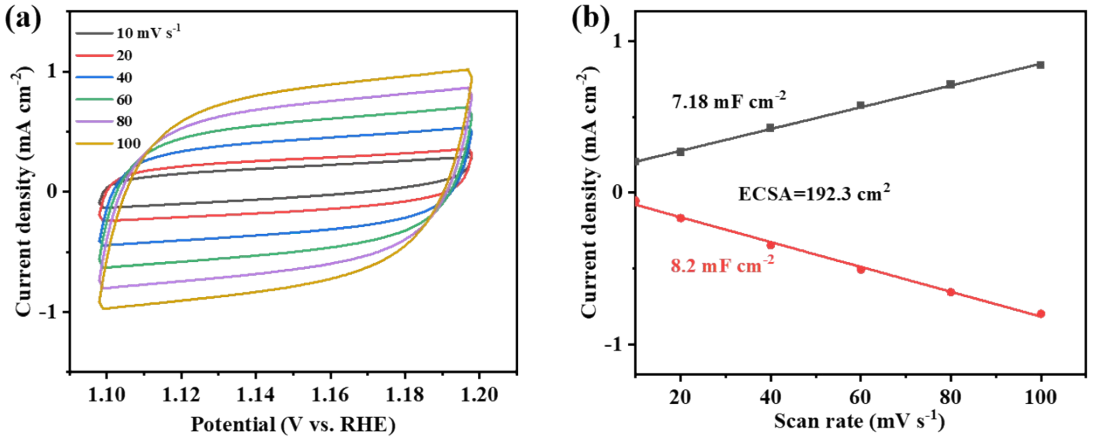

Figure S12. (a) CVs of NG measured in a non-Faradaic region at scan rate of 10 mV s^{-1}, 20 mV s^{-1}, 40 mV s^{-1}, 60 mV s^{-1}, 80 mV s^{-1}, and 100 mV s^{-1}. (b) Capacitive j vs scan rate.

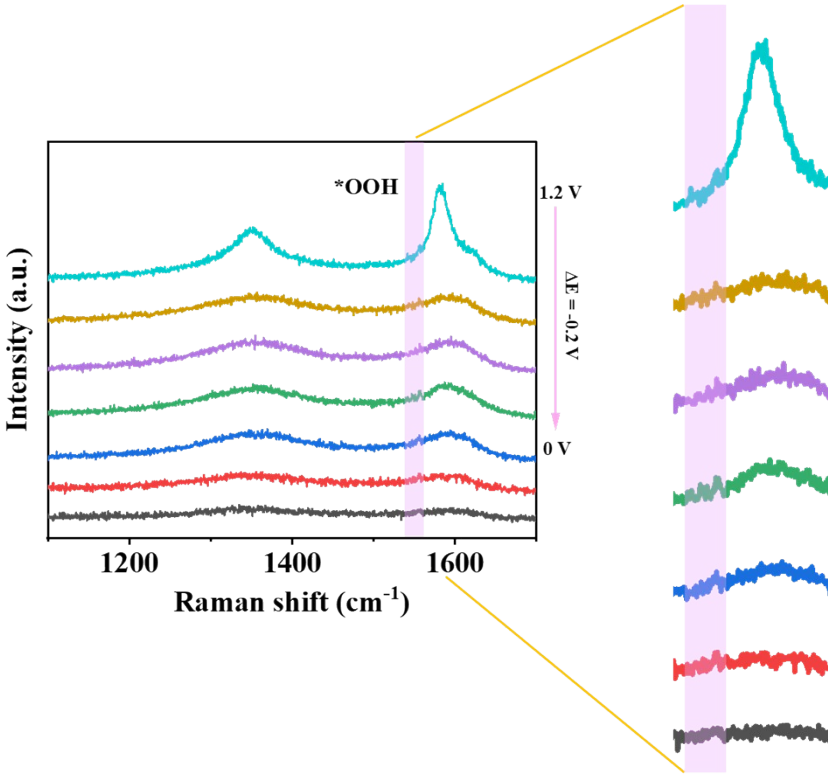

Figure S13. Potential-dependent *in situ* Raman spectra of Zr_3/NG during the ORR process.

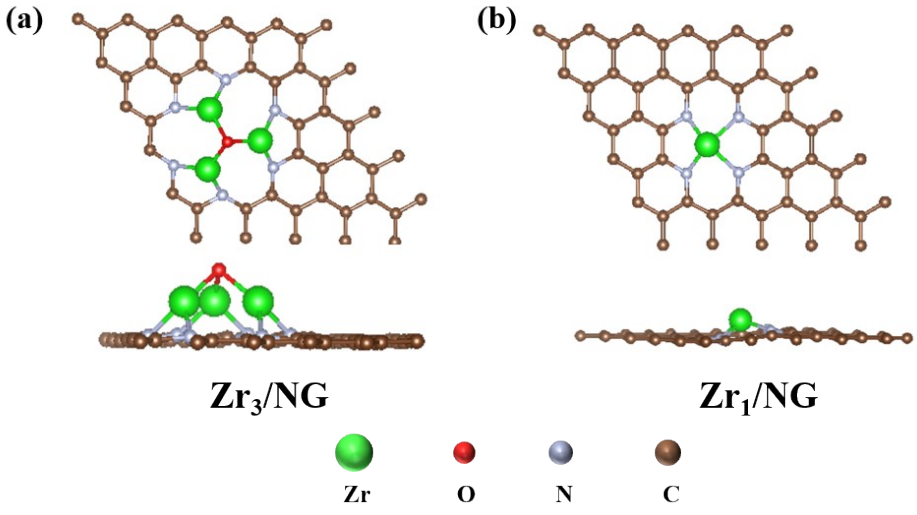

Figure S14. Model schematic diagram of Zr_3/NG (a) and Zr_1/NG (b).

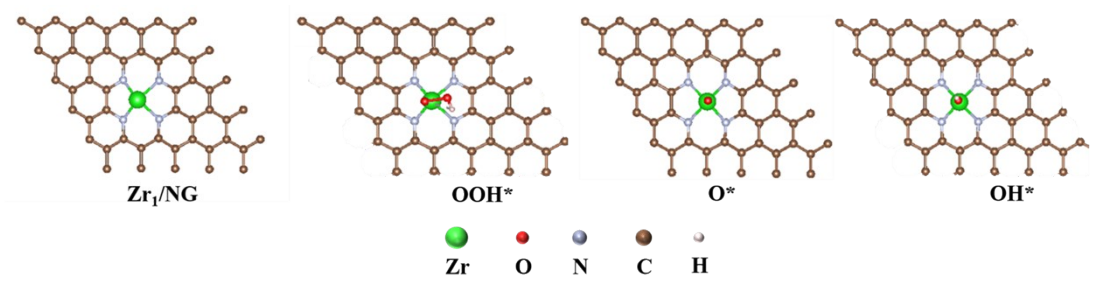

Figure S15. Illustration of ORR process of Zr_1/NG for the adsorption mode of reaction intermediates.

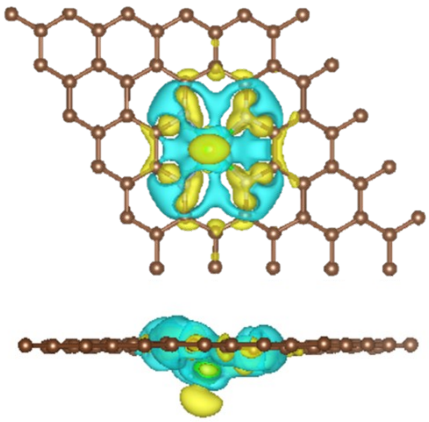

Figure S16. Top and side views of differential charge density of oxygen intermediates adsorbed on Zr_1/NG.

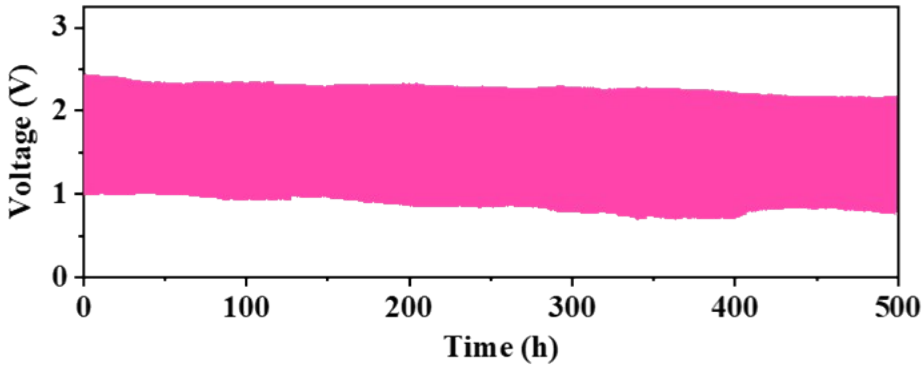

Figure S17. The cyclic stability of Zr_3/NG.

Table S1. Structural parameters extracted from the Zr K-edge EXAFS fitting

Sample	Path	CN	R (Å)	σ^2 (Å^2)	ΔE_0 (eV)	R-factor
Zr_1/NG	Zr-N	4.2±0.1	1.79±0.02	0.005	-1.2	0.02
Zr_3/NG	Zr-N	1.9±0.2	1.82±0.02	0.005	0.8	0.018
	Zr-O	1.1±0.3	1.93±0.03	0.008		
	Zr-Zr	1.9±0.2	3.03±0.03	0.005		

The S_0^2 was fixed at 0.86 (Error ± 0.03). CN is the coordination number. R is the distance between the absorber and the backscattered atom. σ^2 is the Debye-Waller factor. R-factor is the residual factor.

Table S2. ORR comparison of Zr_3/NG with other catalysts

Catalyst	E_{onset} (V vs. RHE)	$E_{1/2}$ (V vs. RHE)	Tafel (mV dec^{-1})	Ref.
Zr_3/NG	**0.987**	**0.857**	**48.2**	**This work**
Co-SA@N-CNFs	-	0.85	50	[2]
Co@WC_{1-x}/NCNTs	0.91	0.81	62.5	[3]
FeCo-N-C	-	0.81	83	[4]
Co_2P/Co_3Fe_7@N–C	-	0.801	99	[5]
Zn-NG-800	-	0.84	50	[6]
FeCo/MoN@NCNTs	-	0.845	84.3	[7]
ZnS@C-2	0.916	0.82	79.8	[8]
TiCN-BCN-Co	-	0.83	90.8	[9]

References

1. W. Gong, H. Arman, Z. Chen, Y. Xie, F. A. Son, H. Cui, X. Chen, Y. Shi, Y. Liu, B. Chen, O. K. Farha and Y. Cui, Highly specific coordination-driven self-assembly of 2D heterometallic metal-organic frameworks with unprecedented johnson-type(J_{51}) nonanuclear Zr-oxocarboxylate clusters, *J. Am. Chem. Soc.*, 2021, **143**, 657-663.
2. S. Zhang, Q. Zhou, L. Fang, R. Wang, T. Lu, Q. Zhao, X. Gu, S. Tian, L. Xu, H. Pang, J. Yang, Y. Tang and S. Sun, Gram-scale synthesis and unraveling the activity origin of atomically dispersed Co-N_4O sites toward superior electrocatalytic oxygen reduction, *Appl. Catal. B Environ.*, 2023, **328**, 122489.

3. J. Cai, X. Zhang, M. Yang, Y. Shi, W. Liu and S. Lin, Constructing $Co@WC_{1-x}$ heterostructure on N-doped carbon nanotubes as an efficient bifunctional electrocatalyst for zinc-air batteries, *J. Power Sources*, 2020, **485**, 229251.

4. X.-G. Wu, R. Wang, F. Ma, X.-L. Liu, D.-L. Jia, H.-C. Yang, Y.-P. Liu, Z.-X. Wang, H.-Z. Zheng, Y.-N. Zhang, J. Hou, J.-J. Huang and S.-L. Peng, FeCo-N encapsuled in nitrogen-doped carbon nanotubes as bifunctional electrocatalysts with a high stability for zinc air batteries, *Rare Metals*, 2023, **42**, 1526-1534.

5. A. Feng, L. Liu, P. Liu, Y. Zu, F. Han, X. Li, S. Ding and Y. Chen, Interfacial nanoparticles of Co_2P/Co_3Fe_7 encapsulated in N-doped carbon nanotubes as bifunctional oxygen electrocatalysts for rechargeable zinc-air batteries, *Mater. Today Energy*, 2024, **44**, 101626.

6. S. Zhang, X. Bai, T. Tang, W. Ruan and J. Guan, Coordination modulation of single-atom Zn sites to boost oxygen reduction performance, *Inorg. Chem. Front.*, 2025, **12**, 2917-2924.

7. Y. Zhang, W. Xue, Y. Ding, J. Chen and X. Xu, FeCo alloy modified MoN electrocatalyst with excellent ORR and OER activities for Zn-air battery, *Inorg. Chem. Commun.*, 2025, **177**, 114374.

8. C. Lin, Y. Yin, G. Wang, X. Cao and J. Ma, Carbon-coated ZnS as

a high-performance ORR/OER bifunctional cathode catalyst for zinc-air batteries, *Int. J. Hydrogen Energy*, 2024, **93**, 221-228.

9. Y. Wang, F. Gu, L. Cao, L. Fan, T. Hou, Q. Zhu, Y. Wu and S. Xiong, TiCN MXene hybrid BCN nanotubes with trace level Co as an efficient ORR electrocatalyst for Zn-air batteries, *Int. J. Hydrogen Energy*, 2022, **47**, 20894-20904.